frontiers | Frontiers in Marine Science

TYPE Original Research
PUBLISHED 27 July 2022
DOI 10.3389/fmars.2022.935609

OPEN ACCESS

EDITED BY
Daniel Rittschof,
Duke University, United States

REVIEWED BY
Mi Zhao,
Temple University, United States
Tara Essock-Burns,
University of Hawaii, United States

*CORRESPONDENCE
Zhe Zheng
zhengzhe@gdou.edu.cn

SPECIALTY SECTION
This article was submitted to Marine Molecular Biology and Ecology, a section of the journal Frontiers in Marine Science

RECEIVED 04 May 2022
ACCEPTED 04 July 2022
PUBLISHED 27 July 2022

CITATION
Xiong X, Cao Y, Li Z, Huang R, Jiao Y, Zhao L, Du X and Zheng Z (2022) Insights from tyrosinase into the impacts of modified morphology of calcium carbonate on the nacre formation of pearl oysters. *Front. Mar. Sci.* 9:935609. doi: 10.3389/fmars.2022.935609

Insights from tyrosinase into the impacts of modified morphology of calcium carbonate on the nacre formation of pearl oysters

Xinwei Xiong[1], Yanfei Cao[1], Zhixin Li[1], Ronglian Huang[1,2,3], Yu Jiao[1,2,3], Liqiang Zhao[1], Xiaodong Du[1,2,3,4,5] and Zhe Zheng[1,2,3]*

[1]Fishery College, Guangdong Ocean University, Zhanjiang, China, [2]Pearl Breeding and Processing Engineering Technology Research Centre of Guangdong Province, Zhanjiang, China, [3]Guangdong Science and Innovation Center for Pearl Culture, Zhanjiang, China, [4]Guangdong Provincial Engineering Laboratory for Mariculture Organism Breeding, Zhanjiang, China, [5]Guangdong Provincial Key Laboratory of Pathogenic Biology and Epidemiology for Aquatic Economic Animals, Zhanjiang, China

Tyrosinase is a type-3 copper protein with six conserved histidine residues within the copper-binding sites. It participates in mollusk nacre formation. Here, we identified nacreous-layer-specific tyrosinases (NLSTyr) from *Pinctada fucata martensii* (*PmTyr-4* and *PmTyr-6*), as well as their homologs in *Pinctada maxima* (*PmaxTyr* and *PmaxTyr4*) and *Pinctada margaritifera* (*PmarTyr* and *PmarTyr-4*), which encoded tyrosinases without the six conserved histidine residues within the copper-binding sites. *PmTyr-4* and *PmTyr-6* mRNAs were spatially concentrated in the mantle central and pearl sac, which are the organs responsible for nacre formation. During shell regeneration and pearl formation, *PmTyr-4* and *PmTyr-6* were also significantly highly expressed in the mantle and pearl sac. RNA interference showed that *PmTyr-4* participated in nacreous-layer formation. The recombinant protein of PmTyr-4 (rPmTyr-4) inhibited the calcium carbonate precipitation rate. Correspondingly, calcium carbonate crystallization assay showed that the aragonite crystals of the rPmTyr-4 group were smaller than those of the control group. Moreover, the calcite and aragonite morphologies of the rPmTyr-4 group were modified compared with the control group. These results suggested that NLSTyr in pearl oyster inhibited calcium carbonate precipitation and affected crystal morphologies during nacre formation. Our findings provided new insights into the evolution and function gain of tyrosinase in Mollusk.

KEYWORDS

tyrosinase, nacre, morphologies, calcium carbonate crystallization, calcium carbonate precipitation

Introduction

Biomineralization is widespread and represents an interdisciplinary research field dealing with the ability of life to form minerals through biologically mediated processes (Song et al., 2019; Ehrlich et al., 2021; Masanja et al., 2022). Biominerals provide a calcification structure and serve as an organ, providing functions including movement, support, and protection, for different organisms (Song et al., 2019; Ehrlich et al., 2021). Mollusk shells and pearls are typical biological minerals attracting the attention of materials scientists and biologists because of their unusual mechanical properties and high economic value (Endo et al., 2018; Yan et al., 2019). A typical shell structure is composed of periostracum, a prismatic layer of calcite crystals, and a nacreous layer of aragonite crystals from the exterior to the interior (Suzuki et al., 2013; Du et al., 2017). Nacre (also known as nacreous layer or mother of pearl) fabricated by mussel, pearl oyster, and some gastropoda species is the main component of shell and pearl. Nacre has excellent combination of strength, stiffness, and toughness, so its formation mechanism is a research focus in the biomineralization field (Levikalisman et al., 2001; Michio and Hiromichi, 2013). More than 95% (w/w) of nacre is calcium carbonate, but organic macromolecules (<5% (w/w)) such as shell-matrix proteins (SMPs) play vital roles in shell formation by forming the organic-matrix framework (Levikalisman et al., 2001; Nudelman et al., 2006; Suzuki and Nagasawa, 2007) and regulating the nucleation, orientation, polymorphism, and morphology of calcium carbonate crystals (Yi et al., 2017; Yang et al., 2019; Yang et al., 2020).

Tyrosinase is the crucial rate-limiting enzyme for melanin biosynthesis (Ando et al., 2007; Kanteev et al., 2015; Huang et al., 2017). It has expanded brilliantly in bivalves (Aguilera et al., 2014; Du et al., 2017). For example, *P. f. martensii* has 53 tyrosinase genes compared with 26 genes in *Crassostrea gigas*, three genes in Lottia gigantea, one in humans, and four in stony coral. Fand is thus an important SMP in nacre (Du et al., 2017; Huang et al., 2017). In mollusk bivalves, studies have outlined the involvement of tyrosinase in the formation of periostracum (Zhang et al., 2006), biogenesis of the initial noncalcified shell (Huan et al., 2013; Miglioli et al., 2019), color formation of the shell (Chen et al., 2017; Zhu et al., 2021), and innate immune system (Zhou et al., 2012; Yu et al., 2021). However, tyrosinases reportedly participate in the shell formation of mollusks because of their high expression levels in calcified tissues and the direct component of SMPs (Zhang et al., 2012; Hüning et al., 2016; Du et al., 2017). For example, in pearl oyster and mussels, tyrosinases have been identified from the shell of their prismatic layer and nacreous layer (Du et al., 2017). The silencing of tyrosinase directly causes the disordered growth of the nacreous layer in *Hriopsis cumingii* (Ren et al., 2020). These results indicate that the expansion of tyrosinases generate novel functions rather than catalysis and directly participates in the formation of calcified shells.

Tyrosinase belongs to type-3 copper protein containing two conserved copper-binding sites (CuA and CuB) with three conserved histidine residues at the CuA and CuB binding sites, respectively, with the identification of tyrosinase genes and tyrosinase crystal structure (Decker et al., 2006; Sendovski et al., 2011; Decker and Tuczek, 2017; Huang et al., 2017; Noh et al., 2020). However, this feature does not seem to be the same in some albino mutants (Jackman et al., 1991; Breimer et al., 1994; Boonanuntanasarn et al., 2004; Liu et al., 2010). In humans, fish, and bacteria, albino phenotypes are caused by mutations in the conserved histidine residues of tyrosinase (Jackman et al., 1991; Breimer et al., 1994; Boonanuntanasarn et al., 2004; Liu et al., 2010). In a previous study, natural mutations of histidine residues within the copper binding site have been observed in tyrosinase sequence of pearl oysters (Aguilera et al., 2014), which has hardly been studied in mollusks. As mentioned above, tyrosinase seems to be directly involved in biomineral generation during shell formation. However, the exact crystallization pathways and mechanisms of tyrosinase (especially for tyrosinases with histidine residue mutation) in shell formation remain largely unknown.

The present study aimed to reveal the functions of nacreous-layer-specific tyrosinase (NLSTyr) in mother-of-pearl formation. We identified NLSTyr from pearl oyster *P. f. martensii* and their homologs in *Pinctada maxima* and *Pinctada margaritifera*. We analyzed the sequence characteristics and structural features of six tyrosinases, as well as the expression patterns of *PmTyr-4* and *PmTyr-6*. We also examined the effect of nacre growth after *PmTyr-4* silencing and detected the effect of novel NLSTyr in calcium carbonate precipitation and calcium carbonate crystallization. The findings can improve our better understanding of the function of nacreous-layer-specific tyrosinase in pearl oysters.

Materials and methods

Experimental materials

Marine bivalves *P. f. martensii* were obtained from Xuwen, Zhanjiang, Guangdong, China. They were cultured in indoor tanks for 4 days before use.

Sequence and expression analysis of tyrosinase gene

The complete sequences of NLSTyr were confirmed through rapid amplification of cDNA ends technology. To obtain the full-length sequence, the 5′- and 3′- end fragments were spliced to the coding sequence by using DNAMAN software. The sequence was analyzed using bioinformatics tools, including open reading framework (ORF) Finder (https://www.ncbi.nlm.

nih.gov/orffinder/), SMART (http://smart.embl-heidelberg.de/smart/show_motifs.pl), Clustal Omega (https://www.ebi.ac.uk/Tools/msa/clustalo/), ProtParam tool (https://web.expasy.org/protparam/), MEGA7 (Version:7.0.21) and evolview (https://evolgenius.info//evolview-v2/#login). The Phyre2 online tool (http://www.sbg.bio.ic.ac.uk/phyre2/protocol) was used to construct the 3D structure, which was then displayed through Chimera (version 1.14).

Total RNA was isolated using TRIzol reagent (Invitrogen, Carlsbad, CA, USA) as previously described (Xiong et al., 2019). The cDNA template was synthesized using oligo (dT)-adaptor, random primer, and M-MLV reverse transcriptase (Promega, USA). Quantitative real-time PCR (qRT-PCR) was performed with three independent replicates by using SYBR Green qPCR mix (Thermo Scientific) on an Applied Biosystems 7500/7500 Fast Real-time system (Applied Biosystems, Foster City, CA, USA). The qRT-PCR was finished under the following program: 5 min at 95°C and 40 cycles (each cycle was for 30 s at 95°C, 15 s at 60°C, and 15 s at 72°C). Gene expression level was calculated through the $2^{(\text{CT }\beta\text{-}actin\text{ - CT Target gene})}$ method with β-actin as the reference gene. Statistical analysis of difference was confirmed by SPSS 22.0 with one-way ANOVA (Duncan-test) or T-test. $P < 0.05$ was considered to be significantly different. All primers used in this study are listed in Table S1 (Supplementary Table S1).

Shell notching and pearl sac production

To test the regular fluctuation of tyrosinase expression levels during shell repair, a shell-notching assay was performed. The pearl oysters were cut with a "V" shaped notch on the shell until it reaches the position of the nacre. At 0 h, mantle pallial and mantle central (MC) were isolated from the untreated pearl oyster. All treated oysters were put back in an indoor tank. The mantle pallial and MC were harvested at 2, 4, 6, 8, 12, 24, 36, 48, 72, 120, and 216 h and immediately immersed in liquid nitrogen. Five samples were collected at each time point.

Host pearl oysters (2 years old) were shade-dried to stimulate the release of gonads 2 weeks prior to nucleus implantation. The implantation procedures were completed by an experienced technician. Mantle grafts (2–3 mm^2) were cut from the donor oyster. Nucleus and mantle graft were implanted into the pearl pocket site of the host oyster's gonad. After surgical implantation, the host pearl oysters were cultured on rafts in offshore waters in Dajing, Xuwen, Zhanjiang, Guangdong, China. Then, eight pearl sacs were collected from the host pearl oysters at 6, 12, and 30 d after transplantation and immediately immersed in liquid nitrogen.

Silencing the expression of *PmTyr-4*

RNA interference (RNAi) experiment was performed to silence *PmTyr-4* expression. Double-stranded PmTyr-4 RNA (ds_PmTyr-4) was prepared with a T7 High-Efficiency Transcription Kit (TransGen Biotech, JT101) and EasyPure RNA Purification Kit (TransGen Biotech, ER701). Sixteen 1.5-year-old oysters were equally divided into two groups. The RNA probes were diluted to 600 μg/μL in diethyl pyro carbonate water and then injected into the adductor muscle of pearl oyster. A total of 100 μL of double-stranded Red Fluorescent Protein RNA (ds_RFP) was injected into the control group. All treated pearl oysters were cultured in the indoor tank and sacrificed 6 days after injection. Mantle tissues were collected, and interference efficiency was confirmed by qRT-PCR. The shells were cut into small sections, washed with ultrapure water, and air dried. The cut shells were observed through scanning electron microscopy (SEM, JSM-6300LV, 15 kV) after coating with gold for 3 min.

Recombinant expression and purification of PmTyr-4

Recombinant PmTyr-4 protein (rPmTyr-4) with maltose-binding protein (MBP) tag was prepared in cooperation with Abmart. *PmTyr-4* coding sequence was inserted into the vector modified from pET30a by Abmart. Then, it was transformed into Rosetta competent cells to express the fusion protein. Transformed cells (OD600 = 0.5–0.8) were induced with 1 mM isopropyl 1-thio-β-D-galactopyranoside (IPTG; Sigma–Aldrich) at 37 °C with 220 rpm for 4 h. Then, the induced cells were collected by centrifuging at 6000 g for 5 min at 4 °C. After washing three times with PBS, the harvested cells were resuspended with PBS and disrupted with an ultrasonic dismembrator at 25% power with 5 s pulse on and 5 s pulse off repetition cycle on ice until the liquid was clear. After centrifugation at 13000 g for 10 min at 4°C, the supernatant was collected and mixed with amylose resin (NEB) at 4°C for 30 min. After washing thoroughly with PBS, the target protein was eluted with 5 mL of elution buffer (10 mM maltose) and desalted by dialysis. The purified protein was analyzed by SDS-PAGE gel. The purified protein concentration was tested using a BCA assay kit (Sangon Biotech, C503051-0500).

Effects of rPmTyr-4 on the formation of calcium carbonate

Calcium carbonate precipitation assay was performed based on the protocol of the research of Fang *et al.* (Fang et al., 2012) with some modifications. In a typical procedure, calcium chloride (100 mM, pH 8.5) and sodium bicarbonate (100 Mm) buffer were prepared. The protein concentration was diluted to 40 μg/mL with ultrapure water. About 10 μL of protein solution was added to 100 μL of calcium chloride buffer, and the mixed solution was transferred to 96-well plates. Finally, 100 μL of

sodium bicarbonate buffer was quickly added to the plates. The absorbance at 570 nm was immediately recorded using a multimode plate reader (EnSpire, PerkinElmer) similar to Fang *et al.* (Fang et al., 2012). The values of absorbance at 570 nm were recorded every minute for 6 min. The experiment was repeated three times. Statistical analysis of difference was confirmed by SPSS 22.0 with T-test and the results were shown as the mean value ± standard deviation (SD).

Calcite and aragonite crystallization is a common assay to simulate biomineralization. *In vitro*, calcite and aragonite crystallization assay was performed to study the effects of rPmTyr-4 on the growth of calcite and aragonite crystals in reference to Yan *et al.* (Yan et al., 2007). 2 μg of MBP was used as control. In a typical procedure, 0.5 g of $CaCO_3$ (Sigma–Aldrich) was dissolved in 50 mL of ultrapure water, and aerated CO_2 gas was bubbled into this solution for 4 h. Excess $CaCO_3$ was removed by passing through 0.22 μm filter unit. The filtrate was aerated with CO_2 gas for another 2 h. About 40 μL of fresh crystallization reaction solution containing 2 μg of rPmTyr-4 protein was added to the cover-glass surface and incubated at 25 °C for 24 h. For aragonite-crystallization assay, in addition to protein, the crystallization reaction solution also contained an additional 50 mM Mg^{2+} which is critical for the formation of aragonite crystals. Finally, the crystallization solution was removed, and the crystals were washed with ultrapure water three times. Raman spectroscopy can identify different crystal types based on photon scattering and the SMP can observe the ultrastructure of the crystal surface. Therefore, the air-dried crystals were characterized by Raman and SEM analyses. The experiment was repeated three times.

Results

Sequence analysis of tyrosinase gene

We cloned six tyrosinase genes from *Pinctada* spp. (Table 1). *PmTyr-4* encoded 478 amino acids with a signal peptide and a tyrosinase domain in *P. f. martensii*. *PmTyr-6* encoded 685 amino acids with a signal peptide and a tyrosinase domain in *P. f. martensii*. *PmaxTyr* encoded 511 amino acids with a tyrosinase domain in *P. maxima*. *PmaxTyr-4* encoded 405 amino acids with a tyrosinase domain in *P. maxima*. *PmarTyr* encoded 821 amino acids with a tyrosinase domain in *P. margaritifera*. *PmarTyr-4* encoded 425 amino acids with a tyrosinase domain in *P. margaritifera*. The sequences of the six cloned tyrosinases were demonstrated in the Figure S1 (Supplementary Figure S1).

Sequence alignment, phylogenetic analysis and tertiary structure of tyrosinase

A total of 54 tyrosinases from 15 mollusks were aligned. The conserved CuA motif $H_{A1}(8/9)H_{A2}XG(6)H_{A3}$ and CuB motif $H_{B1}(3)H_{B2}(15)DPXF(3)H_{B3}$ existed in all bivalves in this study (Figure 1). In *Pinctada* spp., some differences existed in the CuA and CuB motifs in some members of the tyrosinase family due to histidine residue mutation. The CuA motif of PmTyr-4, PmaxTyr-4, and PmarTyr-4 changed to $I_{A1}(7)M_{A2}XG(6)N_{A3}$, whereas the CuA motif of PmTyr-6, PmaxTyr, and PmarTyr changed to $H_{A1}(8)Y_{A2}XG(6)N_{A3}$. The CuB motif of six cloned tyrosinase changed to $Q_{B1}(3)H_{B2}(15)DXXF(3)R_{B3}$. Phylogenetic tree showed that PmTyr-4, PmaxTyr-4, and PmarTyr-4 were in a branches, while PmTyr-6, PmaxTyr, and PmarTyr were in another branches (Supplementary Figure S2). The tertiary structure of 6 cloned tyrosinases showed that the amino acid mutations altered the tertiary conformations of CuA and CuB (Figure 2).

Expression patterns of tyrosinase gene

qRT-PCR was used to detect the relative expression levels of the target genes. The expression levels of PmTyr-4 and PmTyr-6 in eight different tissues: adductor muscle (A), foot (F), gill (GI), hepatopancreas (HE), MC, mantle edge (ME), mantle pallial (MP), and pearl sac (PS) were confirmed (Figure 3). The result presented that PmTyr-4 was significantly highly expressed in MC and PS (Figure 3), which are the organs responsible for the formation of the nacre and pearl, respectively. PmTyr-6 showed relatively higher expression levels in MC, MP, PS, and F (Figure 3).

TABLE 1 The six cloned tyrosinase genes.

Gene ID	Accession number	ORF (bp)	5′-UTR(bp)	3′-UTR(bp)	poly (A)(bp)	pI	MW (kDa)
PmTyr-4	OL310923	1437	58	649	26	8.79	54.76
PmTyr-6	OK482676	2058	146	220	27	8.68	77.46
PmaxTyr	OL551676	1536	145	1198	29	8.1	57.64
PmaxTyr-4	OM210027	1218	196	1009	28	7.62	46.72
PmarTyr	OL739292	2466	12	215	26	8.59	91.53
PmarTyr-4	OM649203	1257	55	–	–	8.48	48.83

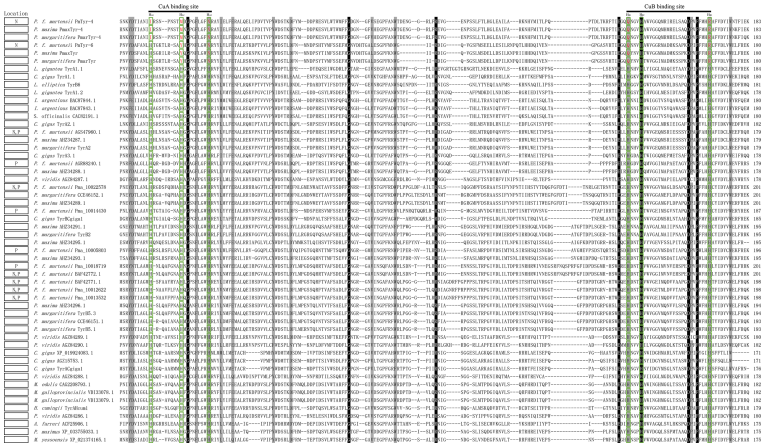

FIGURE 1
Multiple-sequence alignment of members of the tyrosinase family in 15 mollusks. The black background indicates the conserved amino acid; the gray one indicates amino acid with strong similarity. The green box indicates the sites of six conserved histidine residues. Amino acids marked in red in a green box indicate mutated amino acids. N, nacre layer; P, prismatic layer. The full names of the species corresponding with the abbreviations are listed in Table S2 (Supplementary Table S2).

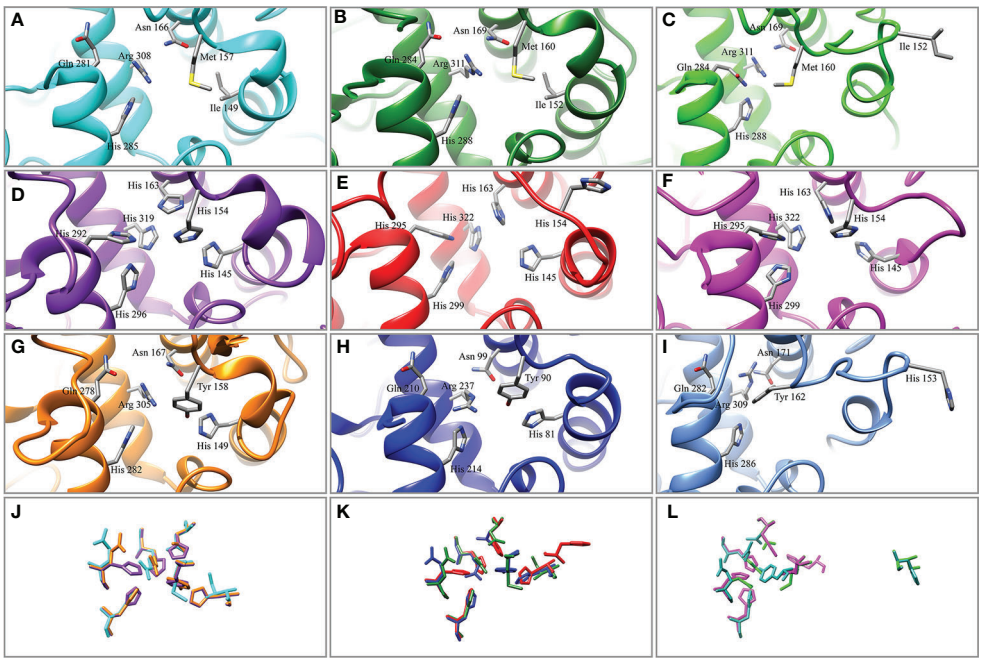

FIGURE 2
Tertiary structure of the copper-binding sites of tyrosinase. **(A)** PmTyr-4. **(B)** PmaxTyr-4. **(C)** PmarTyr-4. **(D)** Tyrosinase-like protein 1 (BAF42771.1). **(E)** Tyrosinase B1.1 (AHZ34289.1). **(F)** Tyrosinase 2 (CCE46152.1). **(G)** PmTyr-6. **(H)** PmaxTyr. **(I)** PmarTyr. **(J)** Structure comparison of copper-binding sites in **(A, D, G)**. **(K)** Structure comparison of copper-binding sites in **(B, E, H) (L)** Structure comparison of copper-binding sites in **(C, F, I)**.

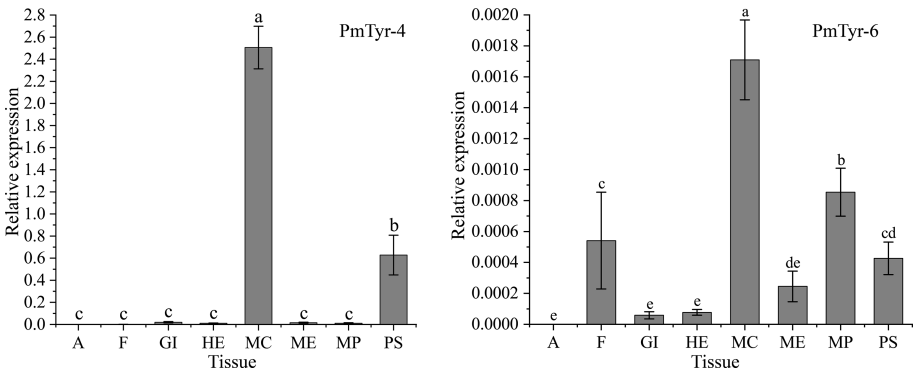

FIGURE 3
Expression patterns of PmTyr-4 and PmTyr-6 in different tissues. A, adductor muscle; F, foot; GI, gill; HE, hepatopancreas; MC, mantle central; ME, mantle edge; MP, mantle pallial; PS, pearl sac. Statistical significance was determined by Duncan-test. Error bars correspond to mean ± SD. Different lower-case letters (a, b, c, and d) were significantly different ($P<0.05$), whereas same ones (a, b, c, and d) were not significantly different ($P>0.05$).

Tyrosinase participated in shell regeneration and pearl formation

A damaged shell can be repaired, which is controlled by mantle tissue and involves shell-mineralization genes (Huang et al., 2019; Xiong et al., 2021). PmTyr-4 presented relatively higher expression levels at 8 and 36–120 h in the MP, and relatively higher expression levels at 36–120 h after shell notching in the MC (Figures 4A, B). The expression levels of PmTyr-6 were significantly upregulated at 12 and 36 h after shell notching in MC (Figure 4C). The formation of pearls, which is similar to shell regeneration, is controlled by the pearl sac and involves SMP genes (Jin et al., 2019; Sato and Komaru, 2019). The expression level of PmTyr-4 in the pearl sac was significantly upregulated at 12 and 30 d (the stage of pearl formation), whereas the expression level of PmTyr-6 in the pearl sac was significantly upregulated at 30 d (Figures 4D, E).

PmTyr-4 participated in nacre formation

The function of PmTyr-4 during nacre formation was analyzed by RNAi technology. In the experimental group, the expression levels of PmTyr-4 in MP and MC were significantly downregulated compared with the control group-injected ds_RFP probe (Figure 5A). Nacre surfaces presented irregular growth compared with the control group (Figure 5B).

Expressed rPmTyr-4 protein

rPmTyr-4 was expressed under 1 mM IPTG induction at 37 °C. MBP-tagged rPmTyr-4 was obtained. The amino acid composition of PmTyr-4 was listed in Table S3 (Supplementary Table S3). Owing to PmTyr-4 containing numerous positively charged residues, the main band of rPmTyr-4 that appeared in the SDS-PAGE gel was about 100 kDa which was a little larger than the predicted molecular mass of 93.11 kDa (53.11 kDa for PmTyr-4 plus 40 kDa for MBP) (Figure 6)

Effects of rPmTyr-4 in calcium carbonate formation

In vitro, the effect of rPmTyr-4 on the precipitation rate of calcium carbonate was revealed by recording the absorbance of the calcium carbonate precipitation system at 570 nm. The absorbance values of the control group were larger than that of the experimental group which showed that rPmTyr-4 inhibited the precipitation rate of calcium carbonate (Figure 7).

In the calcite-crystallization system, Raman spectrum showed that the crystals of the control and experimental groups were calcite, with characteristic peaks at around 154, 280/281, 712, and 1086 cm^{-1} (Figure 8A). The crystals of the control group were regular cuboid crystals, and no obvious change from the typical rhombohedral calcite crystals was found (Figure 8A). Compared with the control group, the edges and corners of calcite crystals in the experimental group presented morphology alteration of contraction (Figure 8A). In the aragonite-crystallization system, Raman spectrum showed that the crystals of the control and experimental groups were aragonite, with characteristic peaks at around 153, 205/206, 705/706, and 1085/1086 cm^{-1} (Figure 8B). The aragonite crystals of the control and experimental groups were spherical (Figure 8B). However, the aragonite surface of the experimental group was shriller than that of the control group (Figure 8B). Additionally, the aragonite crystals of the experimental group were smaller

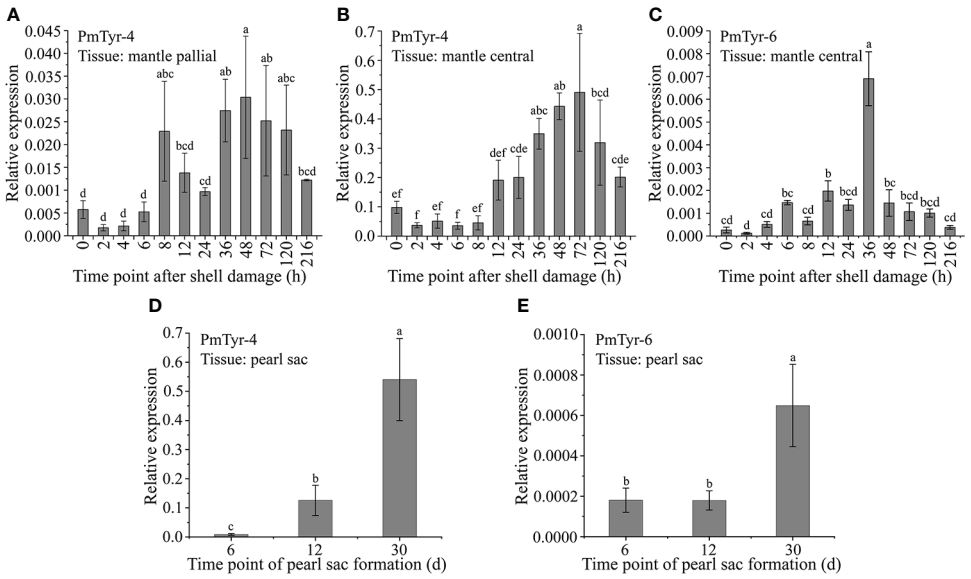

FIGURE 4
Expression patterns of PmTyr-4 and PmTyr-6 during shell regeneration and pearl formation. Statistical significance was determined by Duncan-test. Error bars correspond to mean ± SD. Different lower-case letters **(A–D)** are significantly different (*P<0.05*) and same ones were not significantly different (*P>0.05*). **(A)** The expression level of PmTyr-4 in mantle pallial after shell damage. **(B)** The expression level of PmTyr-4 in mantle central after shell damage. **(C)** The expression level of PmTyr-6 in mantle central after shell damage. **(D)** The expression level of PmTyr-4 in pearl sac after transplantation. **(E)** The expression level of PmTyr-6 in pearl sac after transplantation.

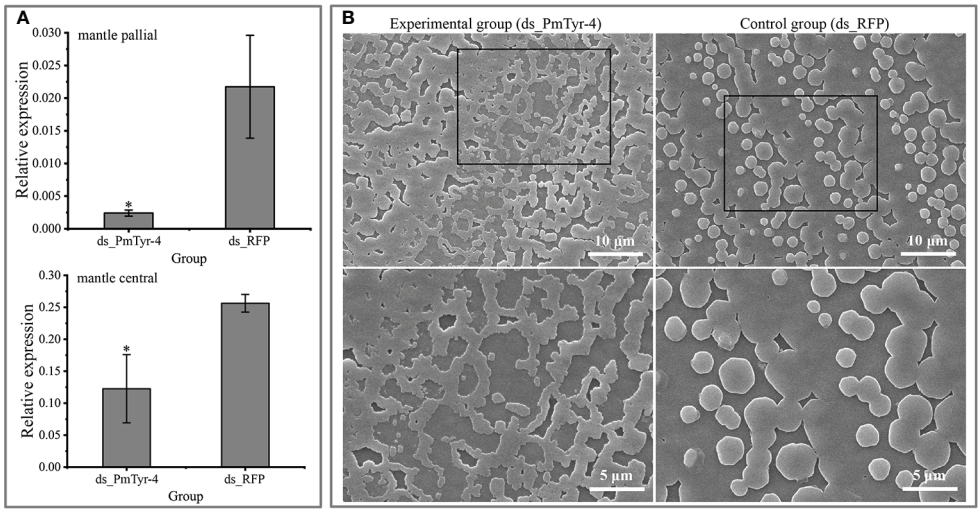

FIGURE 5
Effect of PmTyr-4 on nacre formation. **(A)** Expression levels of PmTyr-4 in MP and MC after RNAi. **(B)** Microstructure of nacre surfaces of the experimental and control groups. * indicates significant difference by T-test (*P<0.05*). Error bars correspond to mean ± SD. The white line in the image indicates the scale.

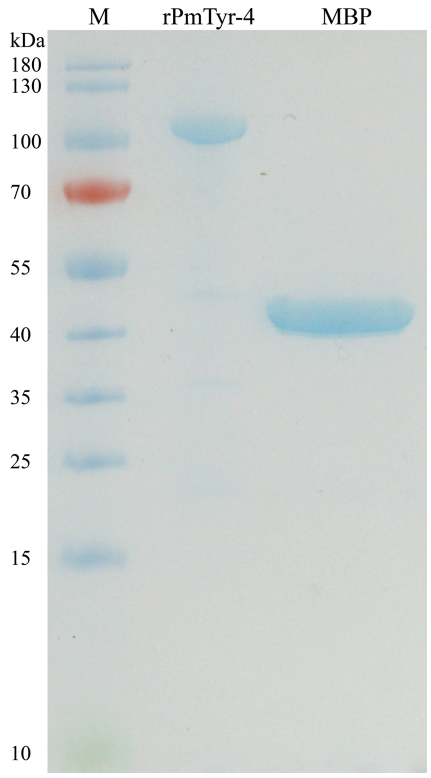

FIGURE 6
SDS-PAGE gel electrophoresis of rPmTyr-4 and MBP protein. M: marker.

than those of the control group (Figure 8B). These findings indicated that rPmTyr-4 did not change the crystal type but modified the crystal shape and inhibited crystal formation.

Discussion

How SMPs construct a matrix framework and how SMPs regulate biomineral deposits is not fully understood. Tyrosinase is a popular SMP with a bivalves-specific expansion (Aguilera et al., 2014; Du et al., 2017; Huang et al., 2017) and plays an important role in shell formation (Zhang et al., 2012; Du et al., 2017; Ren et al., 2020). In our previous study, 12 tyrosinase including 2 NLSTyr's were identified from the shell organic matrix protein in *P. f. martensii* (Du et al., 2017). In this study, we obtained the full-length sequences of the NLSTyr (PmTyr-4 and PmTyr-6). We further cloned their orthologous genes from *P. maxima* (PmaxTyr and PmaxTyr-4), and *P. margaritifera* (PmarTyr and PmarTyr-4). The deduced amino acid sequences of these six cloned genes contained the conserved tyrosinase domain. Tyrosinase is known to contain two conserved copper-binding sites (CuA: H_{A1}(8/9) H_{A2}XG(6)H_{A3} and CuB: H_{B1}(3)H_{B2}(15)DPXF(3)H_{B3}), and six conserved histidine residues within the CuA and CuB motifs are used to coordinate the two copper ions (Decker et al., 2006; Sendovski et al., 2011; Decker and Tuczek, 2017; Huang et al., 2017; Noh et al., 2020). However, the cloned six tyrosinase genes did not encode the six histidine residues within the CuA and CuB motifs. The phenomenon of histidine mutation in tyrosinase has been reported in a previous research (Aguilera et al., 2014). We

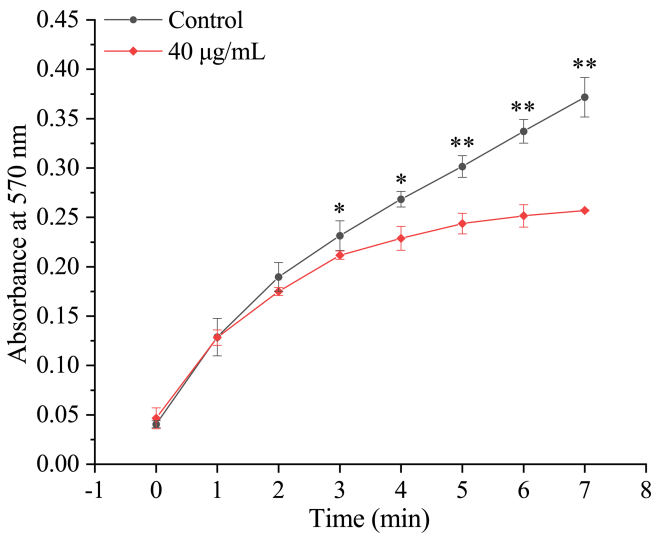

FIGURE 7
Effect of rPmTyr-4 on the precipitation rate of calcium carbonate. ●: 40 μg/mL MBP as control;◆: 40 μg/mL rPmTyr-4. * indicates significant difference by T-test (*P<0.05*). ** indicates extremely significant difference by T-test (*P<0.01*). Error bars correspond to mean ± SD.

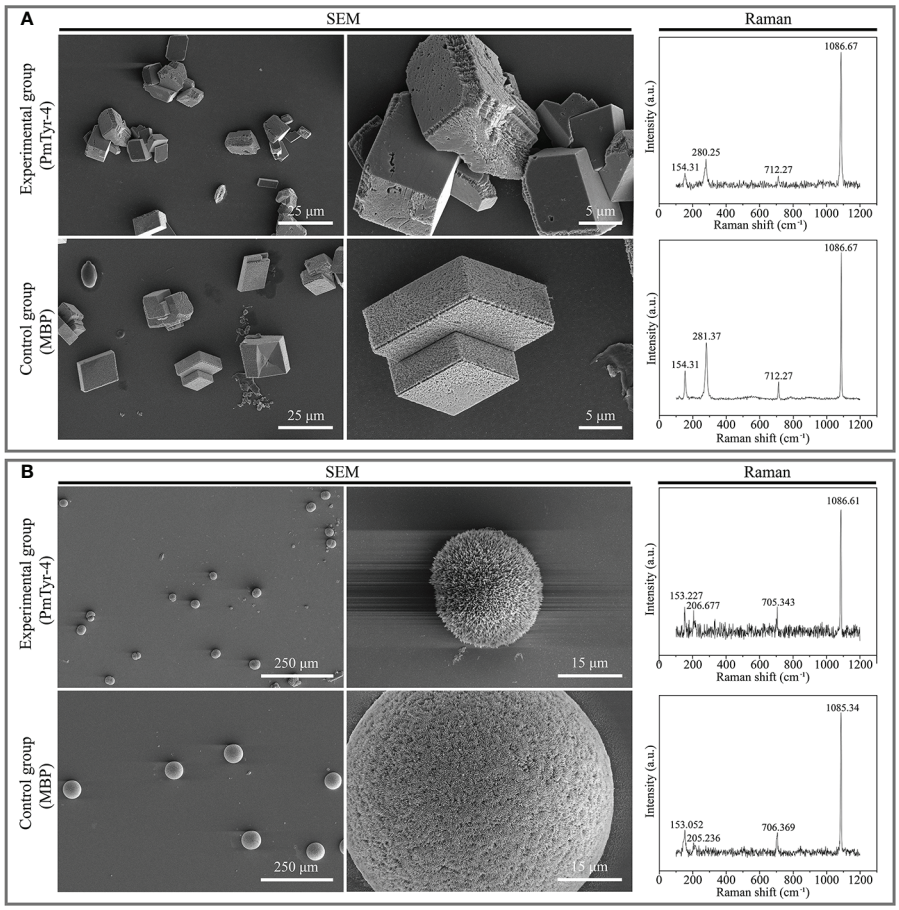

FIGURE 8
Effect of rPmTyr-4 on the crystallization of calcite and aragonite. **(A)** SEM images and Raman identification of crystals in the calcite-crystallization system; **(B)** SEM images and Raman identification of crystals in the aragonite-crystallization system. The white line in the image indicates the scale bar.

found that the mutation of histidine residues occurred specifically in the nacreous-layer-specific tyrosinase in *P. f. martensii*. Among the 15 mollusks, the tyrosinase mutants appeared to be a common feature in *Pinctada* spp. according to the result of multiple sequence alignment. Mutations in the histidine residues of tyrosinase can induce substantial changes in the tertiary structure of proteins, resulting in the loss of copper-ion binding and defective catalytic ability (Jackson and Bennett, 1990; Passmore et al., 1999; Cheng et al., 2006). The tertiary structure of the tyrosinase mutants in *Pinctada* spp. showed a significant change compared with the unmutated tyrosinase, indicating the loss of copper-ion binding ability. We speculated that NLSTyr may have derived new functions in *Pinctada* spp. The SMPs incorporated into the shell are primarily secreted by the mantle tissue (Luke et al., 2011; Endo et al., 2018). Mantle edge and mantle pallial or MC tissues are responsible for the calcification of the prismatic layer and the nacreous layer, respectively (Luke et al., 2011; Endo et al., 2018). By detecting the expression levels of PmTyr-4 and PmTyr-6 in different tissues, we found that their expression levels were the highest in the MC, indicating that they played an important role in the formation of the nacreous layer. Mother of pearl deposition can be observed on the pearl isolated from the pearl sac at 30 d (Mariom et al., 2019). The main biominerals of the pearl and nacreous layer are nacre with a similar formation mechanism (Sato and Komaru, 2019). The highest expression levels of PmTyr-4 and PmTyr-6 in pearl sac were at 30 d after transplantation, indicating their contribution to nacre formation. The similar expression pattern and similar type of mutation within the copper-binding sites indicated a similar function in nacre formation.

We selected PmTyr-4 as the representation to explore the exact crystallization pathways and mechanisms of NLStyrs in pearl oyster. The disordered growth of the nacreous layer caused by the silencing of PmTyr-4 is evidence for its involvement in nacreous-layer formation. We obtained recombinant PmTyr-4 protein through prokaryotic expression *in vitro*. We found that rPmTyr-4 protein visibly inhibited the precipitation of calcium carbonate. This finding

was also illustrated by the fact that the aragonite crystals in the experimental group were smaller than those in the control group. Furthermore, we found that the edges and corners of calcite crystals in the experimental group became more rounded, whereas the surface of aragonite crystals was shriller. This finding indicated that rPmTyr-4 protein obviously altered the morphology of the calcite and aragonite crystals. Previous research has shown that biominerals grew in a controllable and regular manner during shell formation (Yi et al., 2017; Kong et al., 2019). Thus, PmTyr-4 may be used as a guardian against excessive crystal growth and regulate the crystal morphology during shell formation. Previous studies have shown that natural stresses affect biomineralization processes by affecting the physiological activities of mantle tissue (Huang et al., 2019; Zhao et al., 2020; He et al., 2021; Xu et al., 2022). Shell regeneration is controlled by the mantle tissue (Chen et al., 2019; Huang et al., 2019; Xiong et al., 2021). The significantly high expression level of PmTyr-4 at 36-120 h after shell damage indicated its active participation in shell regeneration. Previous studies have shown that the shell repair is an emergency response accompanied by unsynchronized nucleation (Huang et al., 2019), and shell regeneration process accelerate at 36 h after shell damage (Xiong et al., 2021). The high expression of PmTyr-4 during shell regeneration seemed to be contradictory to the requirement of accelerating mineralization. However, it is a common case that inhibitory proteins increase after shell damage (Yi et al., 2017; Yang et al., 2020). Shells are known to be unable grow infinitely and contain amazing regular structures (Kei and Takenori, 2015), which are limited to geometric energy balance and SMPs (Chen et al., 2019; Zhang et al., 2019; Najafkhani et al., 2021). Grain growth is always constrained by grain-boundary dynamics affected by SMPs (Polowczyk et al., 2016; Yi et al., 2017; Zhang et al., 2021). Accordingly, we speculated that PmTyr-4 may affect grain-boundary movement to form well-organized crystals under the requirements of energy balance and growth regulation.

Overall, in the present study, we obtained six tyrosinase genes from *P. maxima*, *P. margaritifera* and *P. f. martensii* that did not encode the six conserved histidine residues within the copper-binding sites. In *P. f. martensii*, PmTyr-4 and PmTyr-6 were nacreous-layer-specific SMPs. PmTyr-4 played crucial role in the formation of mother of pearl by inhibiting calcium carbonate precipitation and modifying crystal morphology. This type of tyrosinase mutants of *Pinctada* spp. may participate in the formation of mother-of-pearl through similar functions. Our results improved our understanding of the function of nacreous-layer-specific tyrosinase in pearl oysters.

Data availability statement

The datasets presented in this study can be found in online repositories. The names of the repository/repositories and accession number(s) can be found in the article/supplementary material.

Author contributions

ZZ and XD conceived the study and developed the research design. XX, RH, YJ, and LZ analyzed the data and participated in the development of the experimental design. XX and YC conducted the experiments, performed the gene expression, conducted the RNA interference experiments, and wrote the manuscript. XX and YC conducted scanning electron microscopy and Raman spectroscopy tests of the shells and crystals. ZL assisted XX and YC in conducting the experiments, sample preparation, and data collection. All authors contributed to the article and approved the submitted version.

Fundings

This work was supported by the National Natural Science Foundation of China (Grant No. 32002369 and 32102817), Science and Technology Program of Guangdong Province (Grant No. 2021B0202020003, 2021A1515011199 and 2020A1515010691), Department of Education of Guangdong Province (Grant No. 2020ZDZX1045 and 2021KCXTD026), China Agriculture Research System of MOF and MARA, and the Guangdong Provincial Special Fund for Modern Agriculture Industry Technology Innovation Teams, Department of Agriculture and Rural Affairs of Guangdong Province (2022KJ146).

Conflict of interest

The authors declare that the research was conducted in the absence of any commercial or financial relationships that could be construed as a potential conflict of interest.

Publisher's note

Supplementary material

The Supplementary Material for this article can be found online at: https://www.frontiersin.org/articles/10.3389/fmars.2022.935609/full#supplementary-material

SUPPLEMENTARY FIGURE 1
Sequences of the 6 cloned tyrosinase. The nucleotide with a frame represents the start and stop codons. Single underlined amino acid sequences are the signal peptide or transmembrane region. Double underlined amino acid sequences are the region of tyrosinase domain. Amino acids marked with gray background are CuA regions. Amino acids marked with gray background and in italics are CuB regions.

SUPPLEMENTARY FIGURE 2
Phylogenetic analysis of mollusk bivalve tyrosinase. *P. f. martensii, Pinctada fucata martensii; P. maxima, Pinctada maxima; P. margaritifera, Pinctada margaritifera; A. farreri, Azumapecten farreri; C. gigas,Crassostrea gigas; H. cumingii, Hyriopsis cumingii; L. gigantea, Lottia gigantea; P. viridis, Perna viridis; P. vulgata, Patella vulgata*. The sequence of tyrosinase genes were came from a previous study (Aguilera et al., 2014).

References

Aguilera, F., McDougall, C., and Degnan, B. M. (2014). Evolution of the tyrosinase gene family in bivalve molluscs: Independent expansion of the mantle gene repertoire. *Acta Biomater.* 10, 3855–3865. doi: 10.1016/j.actbio.2014.03.031

Ando, H., Kondoh, H., Ichihashi, M., and Hearing, V. J. (2007). Approaches to identify inhibitors of melanin biosynthesis via the quality control of tyrosinase. *J. Invest. Dermatol.* 127, 751–761. doi: 10.1038/sj.jid.5700683

Boonanuntanasarn, S., Yoshizaki, G., Iwai, K., and Takeuchi, T. (2004). Molecular cloning, gene expression in albino mutants and gene knockdown studies of tyrosinase mRNA in rainbow trout. *Pigment. Cell Res.* 17, 413–421. doi: 10.1111/j.1600-0749.2004.00166.x

Breimer, L. H., Winder, A. F., Jay, B., and Jay, M. (1994). Initiation codon mutation of the tyrosinase gene as a cause of human albinism. *Clin. Chim. Acta* 227, 17–22. doi: 10.1016/0009-8981(94)90131-7

Cheng, J., Randall, A., and Baldi, P. (2006). Prediction of protein stability changes for single-site mutations using support vector machines. *Proteins.: Structure. Function. Bioinf.* 62, 1125–1132. doi: 10.1002/prot.20810

Chen, X., Liu, X., Bai, Z., Zhao, L., and Li, J. (2017). HcTyr and HcTyp-1 of hyriopsis cumingii, novel tyrosinase and tyrosinase-related protein genes involved in nacre color formation. *Comp. Biochem. Physiol. B-Biochem. Mol. Biol.* 204, 1–8. doi: 10.1016/j.cbpb.2016.11.005

Chen, Y., Liu, C., Li, S. G., Liu, Z. W., Xie, L. P., and Zhang, R. Q. (2019). Repaired shells of the pearl oyster largely recapitulate normal prismatic layer growth: A proteomics study of shell matrix proteins. *ACS Biomater. Sci. Eng.* 5, 519–529. doi: 10.1021/acsbiomaterials.8b01355

Decker, H., Schweikardt, T., and Tuczek, F. (2006). The first crystal structure of tyrosinase: All questions answered? *Angewandte. Chemie. Int. Edition.* 45, 4546–4550. doi: 10.1002/anie.200601255

Decker, H., and Tuczek, F. (2017). The recent crystal structure of human tyrosinase related protein 1 (HsTYRP1) solves an old problem and poses a new one. *Angewandte. Chemie. Int. Edition.* 56, 14352–14354. doi: 10.1002/anie.201708214

Du, X., Fan, G., Jiao, Y., Zhang, H., Guo, X., Huang, R., et al. (2017). The pearl oyster *Pinctada fucata martensii* genome and multi-omic analyses provide insights into biomineralization. *Gigascience* 6, 1–12. doi: 10.1093/gigascience/gix059

Ehrlich, H., Bailey, E., Wysokowski, M., and Jesionowski, T. (2021). Forced biomineralization: A review. *Biomimetics* 6, 46. doi: 10.3390/biomimetics6030046

Endo, K., Kogure, T., and Nagasawa, H. (2018). *Biomineralization* (Berlin: Springer Singapore).

Fang, D., Pan, C., Lin, H., Lin, Y., Zhang, G., Wang, H., et al. (2012). Novel basic protein, PfN23, functions as key macromolecule during nacre formation. *J. Biol. Chem.* 287, 15776–15785. doi: 10.1074/jbc.m112.341594

He, G., Liu, X., Xu, Y., Liang, J., Deng, Y., Zhang, Y., et al. (2021). Repeated exposure to simulated marine heatwaves enhances the thermal tolerance in pearl oysters. *Aquat. Toxicol.* 239, 105959. doi: 10.1016/j.aquatox.2021.105959

Huang, J. L., Liu, Y. J., Jiang, T. F., Dong, W. T., Zheng, G. L., Xie, L. P., et al. (2019). Direct control of shell regeneration by the mantle tissue in the pearl oyster *Pinctada fucata via* accelerating CaCO3 nucleation. *bioRxiv*, 572024. doi: 10.1101/572024

Huang, R., Li, L., and Zhang, G. (2017). Structure-based function prediction of the expanding mollusk tyrosinase family. *Chin. J. Oceanol. Limnol.* 35, 1454–1464. doi: 10.1007/s00343-017-6066-9

Huan, P., Liu, G., Wang, H., and Liu, B. (2013). Identification of a tyrosinase gene potentially involved in early larval shell biogenesis of the pacific oyster *crassostrea gigas*. *Dev. Genes Evol.* 223, 389–394. doi: 10.1007/s00427-013-0450-z

Hüning, A. K., Lange, S. M., Ramesh, K., Jacob, D. E., Jackson, D. J., Panknin, U., et al. (2016). A shell regeneration assay to identify biomineralization candidate genes in *mytilid mussels*. *Mar. Genomics* 27, 57–67. doi: 10.1016/j.margen.2016.03.011

Jackman, M. P., Hajnal, A., and Lerch, K. (1991). Albino mutants of streptomyces glaucescens tyrosinase. *Biochem. J.* 274, 707–713. doi: 10.1042/bj2740707

Jackson, I. J., and Bennett, D. C. (1990). Identification of the albino mutation of mouse tyrosinase by analysis of an *in vitro* revertant. *Proc. Natl. Acad. Sci.* 87, 7010. doi: 10.1073/pnas.87.18.7010

Jin, C., Zhao, J.-Y., Liu, X.-J., and Li, J.-L. (2019). Expressions of shell matrix protein genes in the pearl sac and its correlation with pearl weight in the first 6 months of pearl formation in *hyriopsis cumingii*. *Mar. Biotechnol.* 21, 240–249. doi: 10.1007/s10126-019-09876-z

Kanteev, M., Goldfeder, M., and Fishman, A. (2015). Structure-function correlations in tyrosinases. *Protein Sci.* 24, 1360–1369. doi: 10.1002/pro.2734

Kei, S., and Takenori, S. (2015). Shell microstructure of protobranchia (Mollusca: Bivalvia): Diversity, new microstructures and systematic implications. *Malacologia* 59, 45–103. doi: 10.4002/040.059.0106

Kong, J., Liu, C., Yang, D., Yan, Y., and Zhang, R. Q. (2019). A novel basic matrix protein of *pinctada fucata*, PNU9, functions as inhibitor during crystallization of aragonite. *CrystEngComm* 21, 1250. doi: 10.1039/C8CE02194E

Levikalisman, Y., Falini, G., Addadi, L., and Weiner, S. (2001). Structure of the nacreous organic matrix of a bivalve mollusk shell examined in the hydrated state using cryo-TEM. *J. Struct. Biol.* 135, 8–17. doi: 10.1006/jsbi.2001.4372

Liu, J., Choy, K.-W., Chan, L. W. L., Leung, T.-Y., Tam, P. O. S., Chiang, S. W. Y., et al. (2010). Tyrosinase gene (TYR) mutations in Chinese patients with oculocutaneous albinism type 1. *Clin. Exp. Ophthalmol.* 38, 37–42. doi: 10.1111/j.1442-9071.2009.02220.x

Luke, D. G., David, M., Aaron, W., David, L., and Abigail, E. (2011). Spatial analysis of biomineralization associated gene expression from the mantle organ of the pearl oyster *Pinctada maxima*. *BMC Genomics* 12, 455. doi: 10.1186/1471-2164-12-455

Mariom,, Take, S., Igarashi, Y., Yoshitake, K., Asakawa, S., Maeyama, K., et al. (2019). Gene expression profiles at different stages for formation of pearl sac and pearl in the pearl oyster *Pinctada fucata*. *BMC Genomics* 20, 240. doi: 10.1186/s12864-019-5579-3

Masanja, F., Xu, Y., He, G., Liang, F., Liu, X., Yang, K., et al. (2022). Exploring HSP90 as a biomarker for marine heatwaves in *pinctada maxima*. *Front. Mar. Sci.* 9. doi: 10.3389/fmars.2022.913920

Michio, S., and Hiromichi, N. (2013). Mollusk shell structures and their formation mechanism. *Can. J. Zool.* 91, 349–366. doi: 10.1139/cjz-2012-0333

Miglioli, A., Dumollard, R., Balbi, T., Besnardeau, L., and Canesi, L. (2019). Characterization of the main steps in first shell formation in *mytilus galloprovincialis*: possible role of tyrosinase. *Proc. R. Soc. B.: Biol. Sci.* 286, 20192043. doi: 10.1098/rspb.2019.2043

Najafkhani, F., Kheiri, S., Pourbahari, B., and Mirzadeh, H. (2021). Recent advances in the kinetics of normal/abnormal grain growth: a review. *Arch. Civil. Mech. Eng.* 21, 29. doi: 10.1007/s43452-021-00185-8

Noh, H., Lee, S. J., Jo, H.-J., Choi, H. W., Hong, S., and Kong, K.-H. (2020). Histidine residues at the copper-binding site in human tyrosinase are essential for its catalytic activities. *J. Enzyme Inhib. Med. Chem.* 35, 726–732. doi: 10.1080/14756366.2020.1740691

Nudelman, F., Gotliv, B. A., Addadi, L., and Weiner, S. (2006). Mollusk shell formation: Mapping the distribution of organic matrix components underlying a single aragonitic tablet in nacre. *J. Struct. Biol.* 153, 176–187. doi: 10.1016/j.jsb.2005.09.009

Passmore, L., Kaesmann-Kellner, B., and Weber, B. (1999). Novel and recurrent mutations in the tyrosinase gene and the p gene in the German albino population. *Hum. Genet.* 105, 200–210. doi: 10.1007/s004399900104

Polowczyk, I., Bastrzyk, A., and Fiedot, M. (2016). Protein-mediated precipitation of calcium carbonate. *Materials* 9, 944. doi: 10.3390/ma9110944

Ren, G., Chen, C., Jin, Y., Zhang, G., Hu, Y., and Shen, W. (2020). A novel tyrosinase gene plays a potential role in modification the shell organic matrix of the triangle mussel *hyriopsis cumingii*. *Front. Physiol.* 11. doi: 10.3389/fphys.2020.00100

Sato, Y., and Komaru, A. (2019). Pearl formation in the Japanese pearl oyster (*Pinctada fucata*) by CaCO3 polymorphs: Pearl quality-specific biomineralization processes and their similarity to shell regeneration. *Aquacult. Res.* 50, 1710–1717. doi: 10.1111/are.14057

Sendovski, M., Kanteev, M., Ben-Yosef, V. S., Adir, N., and Fishman, A. (2011). First structures of an active bacterial tyrosinase reveal copper plasticity. *J. Mol. Biol.* 405, 227–237. doi: 10.1016/j.jmb.2010.10.048

Song, X., Liu, Z., Wang, L., and Song, L. (2019). Recent advances of shell matrix proteins and cellular orchestration in marine molluscan shell biomineralization. *Front. Mar. Sci.* 6. doi: 10.3389/fmars.2019.00041

Suzuki, M., and Nagasawa, H. (2007). The structure–function relationship analysis of prismalin-14 from the prismatic layer of the Japanese pearl oyster, *Pinctada fucata*. *FEBS J.* 274, 5158–5166. doi: 10.1111/j.1742-4658.2007.06036.x

Suzuki, M., Nakayama, S., Nagasawa, H., and Kogure, T. (2013). Initial formation of calcite crystals in the thin prismatic layer with the periostracum of *pinctada fucata*. *Micron* 45, 136–139. doi: 10.1016/j.micron.2012.10.010

Xiong, X., Cao, Y., Li, Z., Jiao, Y., Du, X., and Zheng, Z. (2021). Transcriptome analysis reveals the transition and crosslinking of immune response and biomineralization in shell damage repair in pearl oyster. *Aquacult. Rep.* 21, 100851. doi: 10.1016/j.aqrep.2021.100851

Xiong, X., Xie, B., Zheng, Z., Deng, Y., Jiao, Y., and Du, X. (2019). PfmPif97-like regulated by pfm-miR-9b-5p participates in shell formation in *Pinctada fucata martensii*. *PloS One* 14, e0226367. doi: 10.1371/journal.pone.0226367

Xu, Y., Liang, J., He, G., Liu, X., Yang, K., Masanja, F., et al. (2022). Responses of pearl oysters to marine heatwaves as indicated by HSP70. *Front. Mar. Sci.* 9. doi: 10.3389/fmars.2022.847585

Yan, Z., Gu, J., Gong, N., Li, C., Zhou, Y., Xie, L., et al. (2007). N40, a novel nonacidic matrix protein from pearl oyster nacre, facilitates nucleation of aragonite in vitro. *Biomacromolecules* 8, 3597–3601. doi: 10.1021/bm0701494

Yang, X., Yang, D., Yan, Y., Li, S. G., Han, Z. M., Ji, Y. H., et al. (2020). A novel matrix protein PfX regulates shell ultrastructure by binding to specific calcium carbonate crystal faces. *Int. J. Biol. Macromol.* 156, 302–313. doi: 10.1016/j.ijbiomac.2020.04.016

Yang, D., Yan, Y., Yang, X., Liu, J., Zheng, G., Xie, L., et al. (2019). A basic protein, N25, from a mollusk modifies calcium carbonate morphology and shell biomineralization. *J. Biol. Chem.* 294, 8371–8383. doi: 10.1074/jbc.RA118.007338

Yan, W. T., Lau, C. P., Leung, K. M. Y., and Davies, S. N. G. (2019). Problems and prospects of revitalizing marine pearl cultivation in highly urbanized coasts: A case study of tolo harbour in Hong Kong. *Regional. Stud. Mar. Sci.* 31, 100756. doi: 10.1016/j.rsma.2019.100756

Yi, Y., Dong, Y., Xue, Y., Liu, C., Xie, J., Zheng, G., et al. (2017). A novel matrix protein, PfY2, functions as a crucial macromolecule during shell formation. *Sci. Rep.* 7, 6021. doi: 10.1038/s41598-017-06375-w

Yu, F., Lu, Y., Zhong, Z., Qu, B., Wang, M., Yu, X., et al. (2021). Mitf involved in innate immunity by activating tyrosinase-mediated melanin synthesis in pteria penguin. *Front. Immunol.* 12. doi: 10.3389/fimmu.2021.626493

Zhang, G., Fang, X., Guo, X., Li, L., Luo, R., Xu, F., et al. (2012). The oyster genome reveals stress adaptation and complexity of shell formation. *Nature* 490, 49–54. doi: 10.1038/nature11413

Zhang, L., Han, J., Srolovitz, D. J., and Xiang, Y. (2021). Equation of motion for grain boundaries in polycrystals. *NPJ Comput. Mater.* 7, 64. doi: 10.1038/s41524-021-00532-6

Zhang, C., Xie, L. P., Huang, J., Chen, L., and Zhang, R. Q. (2006). A novel putative tyrosinase involved in periostracum formation from the pearl oyster (*Pinctada fucata*). *Biochem. Biophys. Res. Commun.* 342, 632–639. doi: 10.1016/j.bbrc.2006.01.182

Zhang, R., Xie, L., and Yan, Z. (2019). *Biomineralization mechanism of the pearl oyster, pinctada fucata* (Berlin:Springer Singapore).

Zhao, L., Shirai, K., Tanaka, K., Milano, S., Higuchi, T., Murakami-Sugihara, N., et al. (2020). A review of transgenerational effects of ocean acidification on marine bivalves and their implications for sclerochronology. *Estuarine. Coast. Shelf. Sci.* 235, 106620. doi: 10.1016/j.ecss.2020.106620

Zhou, Z., Ni, D., Wang, M., Wang, L., Wang, L., Shi, X., et al. (2012). The phenoloxidase activity and antibacterial function of a tyrosinase from scallop *Chlamys farreri*. *Fish. Shellfish. Immunol.* 33, 375–381. doi: 10.1016/j.fsi.2012.05.022

Zhu, Y., Li, Q., Yu, H., Liu, S., and Kong, L. (2021). Shell biosynthesis and pigmentation as revealed by the expression of tyrosinase and tyrosinase-like protein genes in pacific oyster (*Crassostrea gigas*) with different shell colors. *Mar. Biotechnol.* 23, 777–789. doi: 10.1007/s10126-021-10063-2